

# FIPER: Generalizable Factorized Fields for Joint Image Compression and Super-Resolution

Yang-Che Sun<sup>1</sup> Cheng Yu Yeo<sup>1</sup> Ernie Chu<sup>2</sup> Jun-Cheng Chen<sup>3</sup> Yu-Lun Liu<sup>1</sup>  
<sup>1</sup>National Yang Ming Chiao Tung University <sup>2</sup>Johns Hopkins University <sup>3</sup>Academia Sinica

## Abstract

In this work, we propose a unified representation for Super-Resolution (SR) and Image Compression, termed **Factorized Fields**, motivated by the shared principles between these two tasks. Both SISR and Image Compression require recovering and preserving fine image details—whether by enhancing resolution or reconstructing compressed data. Unlike previous methods that mainly focus on network architecture, our proposed approach utilizes a basis-coefficient decomposition to explicitly capture multi-scale visual features and structural components in images, addressing the core challenges of both tasks. We first derive our SR model, which includes a Coefficient Backbone and Basis Swin Transformer for generalizable Factorized Fields. Then, to further unify these two tasks, we leverage the strong information-recovery capabilities of the trained SR modules as priors in the compression pipeline, improving both compression efficiency and detail reconstruction. Additionally, we introduce a merged-basis compression branch that consolidates shared structures, further optimizing the compression process. Extensive experiments show that our unified representation delivers state-of-the-art performance, achieving an average relative improvement of 204.4% in PSNR over the baseline in Super-Resolution (SR) and 9.35% BD-rate reduction in Image Compression compared to the previous SOTA.

## 1. Introduction

Single Image Super-Resolution (SISR) aims to reconstruct high-quality images from low-resolution counterparts. Specifically, the key lies in accurately restoring fine details and reconstructing the correct arrangement of visual features. Thus, geometric correspondences or repetitive patterns, such as stripes, grids, or textures, are commonly used for evaluation due to their rich details that are crucial to image fidelity. Early CNN-based approaches [21, 46] laid the foundation for SISR, which was later enhanced with GAN-based methods [39] for improved perceptual realism. Follow-up Transformer-based networks [12] address non-

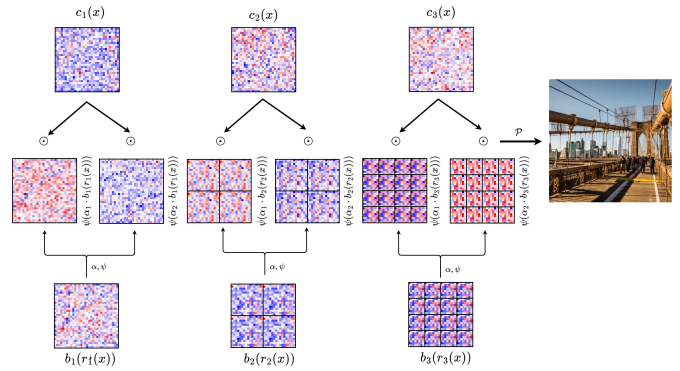


Figure 1. **The Proposed Factorized Fields.** With explicit formulation of repetitive patterns and high frequency components, images can be represented with fine-grained details, especially useful for both Super-Resolution and Image Compression. Note that in this figure  $\alpha = \{1, 16\}$  and  $\psi = \sin$ .

local dependencies, with subsequent Swin Transformer-based approaches sparking tremendous advancements [15, 16, 19], which then inspire more and more complex, delicate designs of heavy network architectures in SISR. However, these prior works have primarily focused on network architecture design rather than addressing the capability of representation. The visual patterns and the inherent nature of image content structure that play an influential role in SISR have not been explicitly considered in the representation learning process. This raises a critical question: beyond a simple network output, can we derive a formulation that more effectively captures these patterns and aligns with the goals of SISR?

On the other hand, image compression serves as a fundamental task in low-level vision applications, where the traditional compression standards [33, 66, 69] lay the groundwork. The emerging learned image compression models [2, 7, 17, 29, 48, 58], compression algorithms of which mostly follow the pixel-space transform coding [7, 27] paradigm, then introduce neural networks to further optimize compression efficiency by learning more compact latent representations and improving reconstruction quality. Specifically, they convert pixels into compact representations through a

transform module, which eliminates the redundancy and reduces the bit cost in the subsequent entropy coding process. However, the core challenge of image compression is to accurately reconstruct the information lost during compression and quantization. In other words, the models are to recover the impaired components in images, which can essentially be viewed as reconstructing a high-quality image from its ‘low-resolution’ version, much like Super-Resolution.

Based on the aforementioned analysis, it becomes clear that although Super-Resolution and Image Compression appear to be two distinct tasks, they share mutual similarities in two key aspects: (1) Both tasks require models to restore fine details from low-quality image content, as well as implicitly capture and reconstruct repetitive structural elements. (2) Both aim to conserve image quality, either by enhancing resolution or efficiently compressing data without significant loss of perceptual fidelity. Hence, inspired by recent advances in decomposition fields and matrices factorization in 3D scene modeling [6, 8–10, 24, 26, 59], we propose a unified representation, **Factorized Fields**, with generalizable Coefficient Backbone and Basis Transformer. This approach explicitly captures multi-scale visual features and repetitive structural components in images through a basis-coefficient decomposition. The resulting representation strikes a balance between being compact and information-rich, enabling the resolution of structural ambiguities and the precise modeling of image details through a multi-frequency formulation. In the meantime, such a formulation imposes a factorization constraint during model training, which not only enhances the quality of single-image super-resolution (SISR) but also reduces distortion and improves compression efficiency by explicitly modeling structural elements. On top of these, to leverage the robust information-recovering capability of SR models, we integrate such priors with Image Compression models, whose knowledge of detail compensation further refines the lost key elements.

Finally, we propose merging the bases by introducing an additional compression branch, consolidating multiple bases into one alongside multi-image transmission. This approach leverages the mutual information across multiple images, reducing the need for redundant transmissions and refining the basis structure. The main contributions of this paper are summarized as follows:

- We propose Generalized Factorized Fields, a unified representation that explicitly models multi-scale visual features and structural components for both super-resolution and image compression.
- We integrate super-resolution with image compression by introducing SR prior during decompression to compensate for lost details and developing a merged-basis compression branch for multi-image compression.
- We demonstrate state-of-the-art performance on bench-

marks for both super-resolution and image compression through extensive experiments.

## 2. Related Works

**Super-Resolution (SR).** Image super-resolution is critical in computer vision, focusing on recovering high-resolution (HR) images from low-resolution (LR) inputs. Following the foundational studies, CNN-based strategies [21, 34, 46, 64, 79] were initially introduced with modeling techniques such as residual learning [18, 40, 45, 47, 68, 77, 78], or recursive learning [16, 65]. Besides, subsequent research also sheds light on GAN-based methods [39, 40, 70, 71] to enhance realism and detail quality. However, the inductive bias of CNN-based networks by restricting spatial locality hinders the capture of long-range dependency from images, which is alleviated by Transformer-based SISR networks [12, 43]. Afterward, SwinIR [44] is proposed to combine spatial locality and non-local information by Swin Transformer [50] with window attention and achieve breakthrough improvement in SISR. Following SwinIR’s success, several works have built upon its framework [19, 75, 80] to reach better image quality as well as solve information bottleneck [18]. Hybrid approaches CRAFT [41] merge the benefits of convolutional and transformer structures to further elevate SR performance. For better feature aggregation, DAT [15] and HAT [13] integrate spatial and channel information using attention mechanisms to enhance their representation capabilities. Moreover, RGT [16] introduces a unique recursive-generalization self-attention mechanism that efficiently captures comprehensive spatial details with a linear increase in computational complexity.

**Image Compression (IC).** Deep learning has significantly advanced image compression, offering superior compression ratios and image quality compared to traditional methods like JPEG [69] and JPEG-2000 [66]. Early CNN-based approaches [3, 7, 28] have been surpassed by transformer-based models [22, 37, 72, 81], which leverage spatio-channel attention for better performance. GAN-based methods [23, 53, 54, 62] have further contributed to real-time adaptive compression. Recently, ELIC [30] introduced efficient compression with unevenly grouped space-channel contextual adaptive coding, while LIC TCM [48] integrated transformers and CNNs to capture both global and local image features. The eContextformer [38] introduced patch-wise, checkered, and channel-wise grouping techniques for parallel context modeling with a shifted window spatial-channel attention mechanism. Grouped-Mixer [42] proposed a transformer-based entropy model with token mixers for inner and cross-group context modeling. Meanwhile, Wavelet Conditional Diffusion [63] introduced a wavelet-based model with uncertainty-aware loss, balancing high perceptual quality with low distortion.

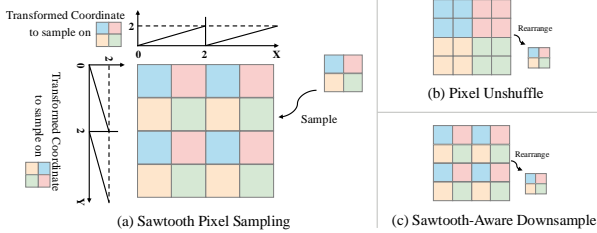


Figure 2. **The correlation between coordinate transformation and downsampling.** (a) The sawtooth transformation example with  $k = 2$ . (b) The PixelUnShuffle downsample. (c) To explicitly model the information for sampling with a sawtooth, we rearrange the feature map in a dilation-like manner in the downsample layer of the Basis Swin Transformer. This way, the feature sampled would capture the information in the original layout correctly; in other words,  $I = \text{Sawtooth-Pixel-Sampling}(\text{Sawtooth-Aware-Downsample}(I))$

In summary, while recent super-resolution and image compression advances focus on increasingly complex architectures, our work takes a different approach. We propose Factorized Fields, a unified framework that models visual and structural features, offering a more comprehensive solution to enhance performance in both tasks.

### 3. Methods

In this section, we present the details of our proposed methods. Inspired by factor fields, which can be formulated by

$$\hat{s}(x) = \mathcal{P}\left(\text{Concat}_{i=1}^N \left\{ c_i(x) \odot b_i(\gamma_i(x)) \right\}\right). \quad (1)$$

and whose details can be found in supplementary materials, we first explain the motivation and how we derive our Factorized Fields for enhanced image reconstruction quality in Sec. 3.1. We then describe how to adapt the formulation to Super-Resolution in Sec. 3.2. Finally, we show how to incorporate such representation with image(s) compression and how we integrate Super-Resolution and Image Compression in Sec. 3.3. Note that the background of learned image compression is described in supplementary materials.

#### 3.1. Formulation of Factorized Fields

As discussed in Sec. 1, the key to superior rendering quality in image regression tasks of both Image Compression and Super-Resolution lies in the capability of the representation to capture accurate structural distribution and fine visual details. Meanwhile, transformations such as Fourier Transform or Wavelet Transform have long been used to model multi-frequency information [25, 36] to express different implicit functions in images; however, such methods often suffer from under-expression due to the pre-defined and limited frequency bands or restriction from its formulation. Thus, we seek a representation that explicitly incorporates and fits multi-scale and multi-frequency components

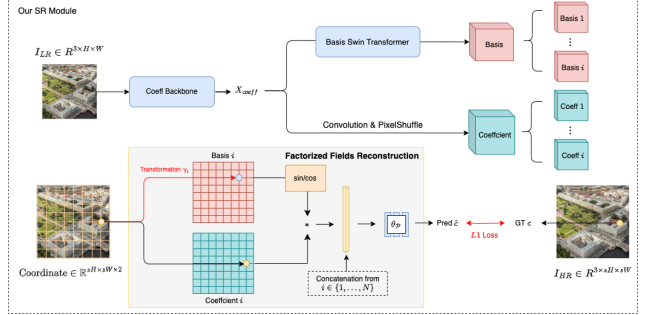


Figure 3. **The overall pipeline of image super-resolution with our Factorized Fields.** Given a low-resolution image  $I_{LR}$ , we first extract coefficient feature map  $X_{\text{coeff}}$  with the coefficient backbone, which is then decoded into coefficient and passed through the basis Swin Transformer for basis, separately. Finally, as in Eq. (4), the coefficient and basis are sampled, multiplied, and decoded for final high-resolution output  $I_{HR}$ , where  $s, H, W$  denote the scale factor, height, and width respectively.

and yet is highly flexible and learnable according to individual features in an image.

Inspired from recent success on such decomposition fields [6, 8–10, 24, 59], we primarily built our Factorized Fields framework on factor fields [10] from Eq. (1):

$$\hat{I}(x) = \mathcal{P}\left(\text{Concat}_{i=1}^N \left\{ c_i(x) \odot b_i(\gamma_i(x)) \right\}\right). \quad (2)$$

Note that  $\hat{I}$  denotes the approximated images, and  $x \in R^2$  are the pixel coordinates.

Such formulation has several key properties: First of all, by decomposing the images into basis frequencies, we can learn the implicit functions of an image and capture the mutual dependencies between pixels and across spatial composition; meanwhile, since the basis and coefficient are specific to every single image and both learnable in all spatial dimensions, the restriction on a limited number of basis (we use  $N = 6$  in all of our experiments) can be alleviated.

A key insight of our work is the use of sawtooth coordinate transformation  $\gamma(x) = x \bmod k, k \in \mathbb{R}$ , which performs best among tested transformations in image regression tasks. The sawtooth transformation maps input coordinates to a periodic space, implicitly capturing patch-like frequency information as shown in Fig. 2a. However, traditional downsampling in neural networks fails to preserve this periodic structure. To address this, we introduce sawtooth-aware downsampling as in Fig. 2c with our Basis Swin Transformer. This rearrangement allows the network to learn correlations between the periodic features in Sawtooth sampling.

Moreover, in practice, we sample the basis via bilinear or bicubic sampling due to memory constraints, *i.e.*, the feature size is less than image height and width, and this poses a severe problem: These nearby sampled pixel features are actually linear or based on cubic interpolation with respect

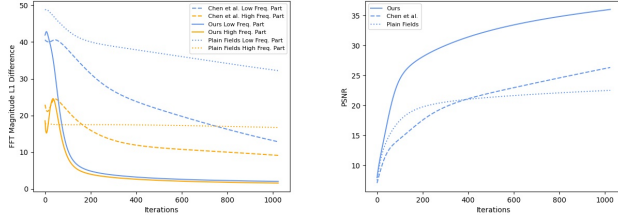


Figure 4. **Comparison of Different Representation** This figure illustrates the performance comparison on a single-image regression task using three different representations: vanilla factor fields in Eq. (1), our Factorized Fields (Eq. (3)), and Plain Fields, which use simple channel-wise tensor concatenation instead of coefficient-basis multiplication. The left panel shows the MAE on the magnitude of different frequency components obtained from the Fourier Transform, while the right panel shows PSNR along training. Although the basis-coefficient decomposition method in [10] yields improvements, it still struggles with slow convergence and inconsistencies between low and high-frequency components. In contrast, by introducing explicit formulations for  $\alpha$  and  $\psi$ , our method aligns different frequency components effectively and achieves superior convergence speed. This advantage becomes especially crucial when the task extends to generalizable applications, such as super-resolution or image compression.

to the basis, and such inductive bias hinders the representation of non-linearity in images. To resolve this, we propose a modified version, our Factorized Fields:

$$\hat{I}(x) = \mathcal{P}\left(\text{Concat}_{i=1}^N \text{Concat}_{j=1}^K \left\{ c_i(x) \odot \psi(\alpha_j \cdot b_i(\gamma_i(x))) \right\}\right), \quad (3)$$

where  $\psi \in \{\sin, \cos\}$ ,  $\alpha_j \in R$ . Here, inspired by the Fourier Series, with a scalar  $\alpha$  which corresponds to an increase in sampling frequency and a transformation function  $\psi$  to add to implicit non-linearity functions and modulation of product, our complete Factorized Fields method stands out by the fact that such formulation significantly enhances the ability to represent complex non-linear structures in images and effectively composes high-frequency components between pixels.

Our Factorized Fields enhance the original Factor Fields [10] in three key ways: (1) **non-linear transformation** through  $\psi \in \{\sin, \cos\}$  enables better modeling of complex image patterns, (2) **multi-frequency modulation** using  $\alpha_j$  allows explicit control over frequency components, and (3) **sawtooth-aware downsampling** preserves periodic structure during feature processing. As shown in Fig. 4, our refined representation contributes to large margin of improvement in convergence and performance, demonstrating the modification is the key to superior information modeling.

### 3.2. Super-Resolution with Factorized Fields

We represent a super-resolved image using our Factorized Fields, where coefficients and basis are generated by networks  $F_{\text{coeff}}$  and  $F_{\text{basis}}$  from a low-resolution Image:

$$\hat{I}_{\text{SR}}(x) = \mathcal{P}\left(\text{Concat}_{i=1}^N \text{Concat}_{j=1}^K \left\{ c_i^{\text{LR}}(x) \odot \psi(\alpha_j \cdot b_i^{\text{LR}}(\gamma_i(x))) \right\}\right), \quad (4)$$

where  $c_i^{\text{LR}}(x) = \text{Conv}(F_{\text{coeff}}(I_{\text{LR}}))_i(x)$  and  $b_i^{\text{LR}}(x) = F_{\text{basis}}(F_{\text{coeff}}(I_{\text{LR}}))_i(\gamma_i(x))$ . Note that we sample the outputs  $\text{Conv}(F_{\text{coeff}}(I_{\text{LR}}))$  and  $F_{\text{basis}}(F_{\text{coeff}}(I_{\text{LR}}))$  with coordinates  $x$  and  $\gamma(x)$ , respectively.

Our model comprises three main components: Coefficient Backbone, Basis Swin Transformer, and Factorized Fields Reconstruction. As shown in Fig. 3, the process begins with  $I_{\text{LR}} \in \mathbb{R}^{3 \times H \times W}$ . The Coefficient Backbone extracts features  $X_{\text{coeff}} \in \mathbb{R}^{C_c \times H_c \times W_c}$ , which are then used to generate coefficients  $c$  through convolution and pixel shuffle operations, and fed into the Basis Swin Transformer to produce a multi-scale basis  $b = \{b_1, \dots, b_N\}$ ,  $b_i \in \mathbb{R}^{C_{b_i} \times H_{b_i} \times W_{b_i}}$ . The coefficients and basis are combined to reconstruct  $I_{\text{SR}} \in \mathbb{R}^{3 \times sH \times sW}$  using Eq. (4), where  $s$  is the scale factor. In our experiments,  $\gamma_i(x)$  is a Sawtooth function:  $\gamma_i(x) = x \bmod k_i$ , with  $k_i \in R$ . We optimize model parameters using an  $L_1$  loss function. To demonstrate our method’s effectiveness, we use existing SR methods [14, 15, 75] as the Coefficient Backbone. For the Basis Swin Transformer, we employ Swin Transformer Blocks [51] with a series of downsampling operations. We use a dilation-like downsampling technique (Fig. 2c) to accommodate the sawtooth sampling pattern. The final basis is refined using additional upsampling and convolution layers.

### 3.3. Image Compression with Factorized Fields and Super-Resolution

Image Compression, at its core, is to strike a balance between the amount of information contained in the latent bits and the final image quality. However, as discussed in Sec. 1, Sec. 2, and Sec. 3.1, most recent works draw emphasis on how to retrieve implicit elements through designing different architectures, such as analysis transforms and entropy models [38, 42], or decompression modules [22, 63], while this paper aims at addressing the representation itself to better capture the structural correlations and thus achieve better image quality through explicit modeling of frequency components and Factorized Fields formulation as in Eq. (3). In addition, with our trained SR model described in Sec. 3.2, it intuitively serves as a strong prior for information recovery, i.e., it contains extensive knowledge of how to reconstruct missing details and enhance image quality by leveraging learned patterns from the training data. Thus, since Super-Resolution and Image Compression share the core principle of reconstructing and enhancing image details from low-quality sources, we can effectively in-

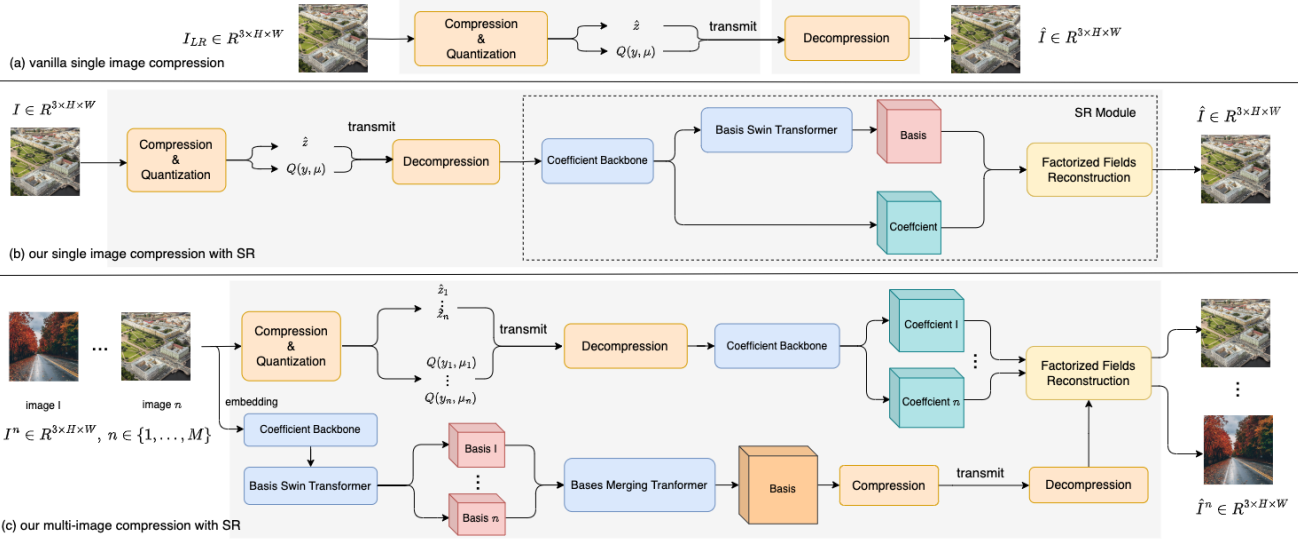


Figure 5. **The illustration of our joint image-compression and super-resolution framework compared with the traditional compression-only method.** (a) Traditional learning-based compression methods. (b) Our approach surpasses (a) by incorporating our Super-Resolution (SR) Module from Sec. 3.2 as information-recovery prior, detailed in Sec. 3.3.1. (c) Expanding on (b), Sec. 3.3.2 introduces a multi-image compression strategy that utilizes both our SR Module and a Basis Merging Transformer to capture shared structure.

tegrate this prior into the compression pipeline. In the following, we respectively present the proposed joint framework for the single and multi-image compression tasks.

### 3.3.1. Single Image Compression

The overall pipeline is shown in Fig. 5b. To demonstrate the robustness of our representation and the effectiveness of the SR prior, the compression and decompression networks greatly follow [48], with only the synthesis transform replaced by our SR pipeline, where the details can be referenced in Supplementary Materials. In practice, the training is performed in two stages. After we obtain the trained SR prior, the model is fine-tuned with a lower learning rate alongside the compression module, which is then trained end-to-end with the loss function defined as

$$L = R(\hat{y}) + R(\hat{z}) + \lambda \cdot D(x, \hat{x}), \quad (5)$$

### 3.3.2. Multi-Image Compression

For each basis  $b_i \in R^{C_{b_i} \times H_{b_i} \times W_{b_i}}$  associated with any arbitrary image, we can consider it as encapsulating the inherent pixel structure. These bases can be combined into a unified generic basis that captures the structural distribution of images and potentially reduces noise. Given  $M$  images and their respective bases  $b_i^n, n \in \{1, \dots, M\}$ , we apply a Basis Merging Transformer  $F_{\text{merge}}$  at each location to integrate the  $M$  elements:

$$b_i(h, w) = F_{\text{merge}}(\{b_i^n(h, w) \mid n \in 1, \dots, M\}), \quad (6)$$

where  $0 \leq h < H_{b_i}$ ,  $0 \leq w < W_{b_i}$ ,  $F_{\text{merge}}$  is a standard transformer, similar in architecture to that described in [60].

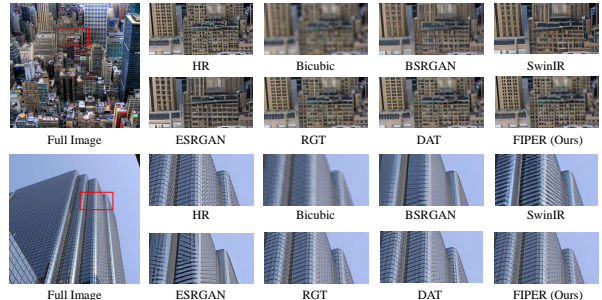


Figure 6. **Visual comparisons on super-resolution (4 $\times$ ).**

We treat the bases as tokens and prepend the sequence with a  $CLS$  token, concluding the sequence to form the final merged basis.

Since compression induces error, according to Fig. 5b, the Coefficient feature map  $X_{\text{coeff}}$  generated with Coefficient Backbone contains misinformation, and Basis Swin Transformer that uses such features would capture the information wrongfully for the basis and thus amplify error. To solve this, we exploit the mergeable property of basis, compress and transmit the merged basis independently along other quantized variables  $\{Q(y, \mu), \hat{z}\}$ , and finally reconstruct the  $M$  images with the merged basis and their individual decoded coefficients. as illustrated in Fig. 5c. This way, we can enjoy less information loss with basis while maintaining low bit rates.

Table 1. **Quantitative comparisons on  $4\times$  super-resolution with state-of-the-art methods.** The best results are colored **red**. The models with † are those who use same-task pretraining [14]. Please refer to **quantitative results** in Sec. 4.1 for details.

Method	Params	MACs	Forward Pass	Set5		Set14		B100		Urban100		Manga109	
	(M)	(G)	Memory (MB)	PSNR↑	SSIM↑	PSNR↑	SSIM↑	PSNR↑	SSIM↑	PSNR↑	SSIM↑	PSNR↑	SSIM↑
SwinIR [44](ICCV2021W)	28.01	119.68	3,826	32.93	0.9043	29.15	0.7958	27.95	0.7484	27.56	0.8273	32.22	0.9273
ATD [76](CVPR2024)	20.26	77.10	6,572	33.14	0.9061	29.25	0.7976	28.02	0.7524	28.22	0.8414	32.65	0.9308
DAT [15](ICCV2023)	14.80	61.66	4,192	33.15	0.9062	29.29	0.7983	28.03	0.7518	27.99	0.8365	32.67	0.9301
RGT [16](ICLR2024)	13.37	834.25	3,404	33.16	0.9066	29.28	0.7979	28.03	0.7520	28.09	0.8388	32.68	0.9303
HAT† [13](CVPR2023)	20.77	86.02	3,692	33.18	0.9073	29.38	0.8001	28.05	0.7534	28.37	0.8447	32.87	0.9319
HAT-L† [13](CVPR2023)	40.84	167.27	6,804	33.30	0.9083	29.47	0.8015	28.09	0.7551	28.60	0.8498	33.09	0.9335
ATD-L*	49.42	184.83	15,582	33.12	0.9062	29.31	0.7985	28.02	0.7514	28.25	0.8422	32.78	0.9309
DAT-L*	43.01	175.42	11,326	33.33	0.9084	29.40	0.8009	28.04	0.7543	28.49	0.8473	33.02	0.9321
ATD-F† (Ours)	45.46	149.87	8,674	33.29	0.9082	29.48	0.8017	28.03	0.7539	28.53	0.8487	33.11	0.9335
DAT-F† (Ours)	40.00	134.42	6,206	33.45	0.9094	29.60	0.8039	28.13	0.7560	28.75	0.8520	33.23	0.9339
HAT-F† (Ours)	45.97	158.79	5,750	33.53	0.9100	29.65	0.8050	28.18	0.7569	28.79	0.8527	33.33	0.9342
HAT-F-ImageNet† (Ours)	45.97	158.79	5,750	33.55	0.9102	29.63	0.8049	28.18	0.7569	28.80	0.8529	33.33	0.9342
HAT-L-F† (Ours)	66.04	240.03	8,888	<b>33.75</b>	<b>0.9116</b>	<b>29.87</b>	<b>0.8091</b>	<b>28.31</b>	<b>0.7597</b>	<b>29.51</b>	<b>0.8637</b>	<b>33.36</b>	<b>0.9343</b>
HAT-F-Basis-First† (Ours)	46.67	161.66	5,696	33.33	0.9085	29.47	0.8015	28.10	0.7554	28.57	0.8494	33.14	0.9336
HAT-F-Concat† (Ours)	45.52	129.05	4,826	33.46	0.9095	29.57	0.8035	28.16	0.7566	28.73	0.8518	33.28	0.9341

## 4. Experiments

### 4.1. Image Super-Resolution

**Experimental Setup.** We conduct extensive experiments to validate the effectiveness of our Factorized Fields representation for Super-Resolution tasks. Following the strategy outlined in [13] and [18], we adapt the same-task pretraining approach for all the Super-Resolution models. Unlike these previous works, we leverage the SA-1B dataset from [35], which includes approximately 10 million images, where we randomly sample 4 million for training, which is much less than that of ImageNet [20], which is used for [13] and [18] pretraining. Note that we use SA-1B just for its content-rich and high-resolution images since SA-1B is designed for training segmentation models, whereas ImageNet focuses primarily on single-class prediction. We further conduct experiments to compare training performance with SA-1B and ImageNet in Tab. 1. While the performances are mostly equivalent, we witness faster convergence with SA-1B during training.

To be more focused on the representation itself, we utilize various pre-trained SR models (SwinIR [44], HAT [14], DAT [15], and ATD [76]) as the Coefficient Backbone, with a consistent Basis Transformer architecture. Training involves initializing the Coefficient Backbones from pre-trained SR models and randomly initializing the Basis Transformers. Models are pre-trained for 300k iterations on the SA-1B dataset. After pretraining, we use DF2K (DIV2K [1] + Flickr2K [46]) as the finetuning dataset following [13, 19] for 200k iterations.

For pretraining, we utilize AdamW optimizer with learning rate  $1e-4$ , batch size 16, betas (0.9, 0.99), and other parameters set to PyTorch default, while we use learning rate

$1e-5$  during finetuning. Throughout training, the input is randomly cropped to  $256 \times 256$  and bicubically resized to  $64 \times 64$  for Coefficient Backbone input. As for the hyperparameter of Factorized Fields, the number  $N$  of coefficient and basis is set to 6, and the scalars  $\alpha_j$  are set to  $\{1, 4, 16, 64\}$  since we want to capture both base frequency  $\alpha_j = 1$  and high frequency  $\alpha_j = 64$  information. More implementation details can be found in supplementary materials.

**Quantitative Results.** Tab. 1 presents the quantitative comparison between our approach and state-of-the-art (SoTA) methods. We evaluate the methods using five benchmark datasets, including Set5 [5], Set14 [74], BSD100 [55], Urban100 [31], and Manga109 [56]. For quantitative metrics, PSNR and SSIM are reported. The average relative improvement of **204.4%** in PSNR over the baseline across the five datasets is calculated using the formula  $(c - b)/(a - b)$ , where  $b$  represents the PSNR of a representative baseline, SwinIR,  $a$  represents the PSNR of SOTA, HAT-L, and  $c$  represents the PSNR of our best model, HAT-L-F. This formula measures the relative performance gain of our model compared to the gap between HAT-L and SwinIR.

To validate the effectiveness of our framework, we employ three different SoTA SR models—ATD [75], DAT [15], and HAT [14]—as the Coefficient Backbone in our pipeline, which we denote as ATD-F, DAT-F, and HAT-F, respectively. These models exhibit significant improvements when compared to their counterparts ATD-L, DAT-L, and HAT-L, which possess similar parameter counts. It is important to note that only [14] provides a large-scale model. To maintain fairness, we scale up ATD and DAT to match this size and train them under the same configuration

as our model, including both pretraining and fine-tuning stages. To ensure an equitable comparison with other methods, we further train another model, HAT-F-ImageNet, using ImageNet as the pretraining dataset, following the protocols outlined in [12, 14]. The results demonstrate that its performance remains consistent with only minor perturbations.

Furthermore, in traditional Fourier Series and other image processing methods [69], the basis is typically derived first and then used to compute the coefficients. In contrast, our method derives the coefficient features first, as illustrated in Fig. 3. To explore this difference, we develop another variant of our model, denoted HAT-F-Basis-First, where we reverse the order of operations. In this case, we first pass the image through the Basis Swin Transformer and then use the resulting basis features and the image input to derive the coefficients. This approach, however, leads to a gigantic performance drop, showing the importance of the order of the pipeline. Specifically, we argue that in our pipeline, the Coefficient Backbone functions more as a feature extraction module, where the refined features facilitate downstream basis extraction.

Lastly, to evaluate the effectiveness of our Factorized Fields, we trained a model named HAT-F-Concat, which does not apply the formulation in Eq. (3). Instead, it concatenates the basis and coefficient directly and decodes the resulting features to produce the output. Although this approach results in reduced performance, which indicates the representation does act as an imperative role in modeling image information, the Basis Swin Transformer with Sawtooth downsampling still contributes to improved reconstruction, even without Factorized-Fields decoding, highlighting its effectiveness.

**Visual Comparison.** We provide the visual comparison in Fig. 6. The images are randomly sampled from the DIV2K dataset. Our method faithfully reconstructs the image details, whereas the other approaches suffer from over-smoothing or hallucinating details absent in the ground truth.

**Multi-frame SR.** Due to the space limit, we provide additional comparisons on multi-frame SR in the supplementary materials.

## 4.2. Single- and Multi-Image Compressions

**Experimental Setup.** We evaluate our Factorized Fields representation for image compression tasks, comparing it against state-of-the-art methods. Following our Super-Resolution setting in Experiment Setup from Sec. 4.1, we use the same set of SA-1B for training. To emphasize our representation, we initialize compression and decompression modules in Fig. 5 from pre-trained [48] and the SR Module from those in Sec. 4.1, we then train the pipeline

Method	BD-Rate (%) ↓	Latency(s)		Params(M)
		Tot Enc ↓	Tot Dec ↓	
VTM	0.00	129.21	0.14	-
Xie (MM 21')	-0.78	2.93	6.00	50.0
Cheng (CVPR 22')	5.44	1.98	4.69	29.6
STF (CVPR 22')	-4.31	0.14	0.13	99.9
ELIC (CVPR 22')	-7.24	0.07	0.09	36.9
TCM (CVPR 23')	-11.74	0.16	0.15	76.7
TCM-HAT-L-F (Ours)	-21.09	0.109	0.264	110.34
TCM-HAT-F-multi M=1 (Ours)	27.96	0.232	0.174	131.35
TCM-HAT-F-multi M=2 (Ours)	2.70	0.232	0.174	131.35
TCM-HAT-F-multi M=4 (Ours)	-10.11	0.232	0.174	131.35
TCM-HAT-F-multi M=8 (Ours)	-16.61	0.232	0.174	131.35
TCM-HAT-F-multi M=16 (Ours)	-19.88	0.232	0.174	131.35
TCM-HAT-F-multi M=24 (Ours)	-20.97	0.232	0.174	131.35

Table 2. **Comprehensive evaluation for image compression.** Using VTM as an anchor for calculating BD-Rate. Latencies are measured under an NVIDIA GTX 3090 GPU.

end to end on 256x256 patches for 200k iterations, with AdamW optimizer [52] with learning rate 1e-5, batch size 16, betas (0.9, 0.99) and other parameters set to PyTorch default.

We integrate our SR Module with the pre-trained compression module TCM, creating TCM-HAT-F and TCM-HAT-L-F models. TCM-HAT-F-multi represents the multi-image compression pipeline. For multi-image compression in Fig. 5.c, we set the Basis Swin Transformer and the Basis Merging Transformer to be trainable while the other parts remain frozen.

**Rate-Distortion Performance Comparison.** We compare our model with State-of-the-Art learned end-to-end image compression algorithms, including [49], [11], [82], [73], [17], [2], [42], [32], [57], [4], [61], and [30]. The classical image compression codec, VVC [67], is also tested by using VTM12.1. The rate-distortion performance on various datasets, including Kodak, Tecnick’s old test set with resolution 1200x1200, and CLIC Professional Validation, is shown in Fig. 7.

In Tab. 2, our TCM-HAT-L-F model achieved a significant BD-Rate improvement of -21.09% compared to VTM, outperforming previous state-of-the-art methods. The multi-image compression approach (TCM-HAT-F-multi) shows increasing performance gains with the number of images compressed simultaneously, reaching -20.97% BD-Rate improvement for  $M = 24$ . The result shows that direct transmission of bases would reduce the error from Coefficient Backbone to Basis Swin Transformer and that the distortion increases with  $M$ , as the information contained in the merged basis is limited, and merging multiple bases into one would cause increasing information loss.

Our analysis reveals several significant advantages of the FIPER framework in image compression tasks. The approach demonstrates substantial improvements in compression efficiency across various benchmark datasets, including Kodak, CLIC, and Tecnick, indicating its broad applicability. Notably, the multi-image compression strategy

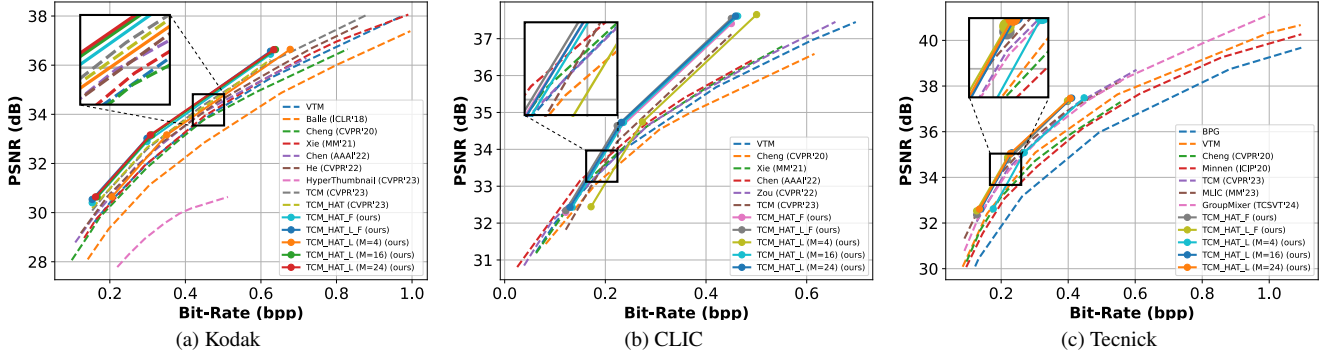


Figure 7. Performance (RD-Curve) evaluation on image compression using different datasets.

Method	Kodak						CLIC						Tecnick					
	$\lambda = 0.0025$		$\lambda = 0.0067$		$\lambda = 0.025$		$\lambda = 0.0025$		$\lambda = 0.0067$		$\lambda = 0.025$		$\lambda = 0.0025$		$\lambda = 0.0067$		$\lambda = 0.025$	
	bpp	PSNR $\uparrow$	bpp	PSNR $\uparrow$	bpp	PSNR $\uparrow$	bpp	PSNR $\uparrow$	bpp	PSNR $\uparrow$	bpp	PSNR $\uparrow$	bpp	PSNR $\uparrow$	bpp	PSNR $\uparrow$	bpp	PSNR $\uparrow$
TCM[48]	0.1533	30.0834	0.2983	32.5841	0.6253	36.1345	0.1214	31.8207	0.2235	34.2098	0.4503	37.1201	0.1268	32.0588	0.2193	34.3669	0.3981	36.9066
TCM-HAT-F-Scratch	0.1570	30.0857	0.2976	32.5893	0.6211	36.1389	0.1214	31.9421	0.2235	34.2894	0.4503	37.1434	0.1258	32.0632	0.2189	34.3781	0.4001	36.9223
TCM-HAT	0.1567	30.1843	0.2992	32.6454	0.6268	36.2267	0.1220	31.9737	0.2266	34.3319	0.4512	37.2486	0.1262	32.1423	0.2174	34.5124	0.3971	36.9934
TCM-HAT-F	0.1574	<b>30.4012</b>	0.2998	<b>32.8910</b>	0.6276	<b>36.4461</b>	0.1229	<b>32.1917</b>	0.2249	<b>34.4109</b>	0.4512	<b>37.3135</b>	0.1255	<b>32.4591</b>	0.2186	<b>34.7656</b>	0.3975	<b>37.3244</b>

Table 3. Validation of the effectiveness of SR prior. The best PSNRs are marked in red.

Metric	PSNR $\uparrow$	SSIM $\uparrow$	LPIPS $\downarrow$
Baseline [10]	22.04	0.505	0.5296
Ours	38.44	0.999	0.0385
No $\psi$ to control magnitude	13.46	0.147	0.766
No $\alpha$ for pixel-wise frequency information	21.25	0.537	0.527

Table 4. Comparison of improvements of Factorized Fields.  $\psi$  and  $\alpha$  are the same in Eq. (4).

shows particularly promising results for larger image sets, suggesting scalability benefits. Furthermore, our method maintains competitive latency while significantly improving compression performance and balancing efficiency and quality.

### 4.3. Ablation Studies

**Influence of SR Priors in Image Compression.** We conduct experiments with various configurations to verify the proposed image compression pipeline’s effectiveness. As shown in Tab. 3, we present the quantitative performance of models trained with different values of  $\lambda$  in Eq. (5). Specifically, TCM-HAT refers to substituting our SR Module with the original HAT [14] in the pipeline illustrated in Fig. 5b. TCM-HAT-F represents our complete pipeline, while TCM-HAT-F-Scratch denotes the same pipeline but with the SR Module initialized randomly. Our results demonstrate that integrating SR priors with image compression improves performance, and our proposed representation further enhances results. This highlights the robustness of our Factorized Fields in capturing fine details in image regression tasks.

**Effectiveness of Factorized Fields Design.** We conduct experiments to verify our modification of Factorized Fields, modified from Eq. (1) to Eq. (3). The quantitative performance reported on single-image regression is shown in Tab. 4, where each result is measured after 256 iterations. Compared to baseline results, our refinements in modeling pixel-level frequency have significantly improved all performance metrics. Additionally, our results demonstrate that the modulation function  $\psi$  and the scalar  $\alpha$  are interdependent, each essential to the other’s function.

## 5. Conclusion

We proposed Factorized Fields, a representation that models implicit structures and patterns by decomposing images into multi-frequency components. This approach addresses challenges in Super-Resolution and Image Compression by restoring details and preserving visual fidelity. We integrate SR priors with Image Compression for improved information recovery and introduce a basis merging technique for enhanced rendering quality across multiple images. Experiments demonstrate state-of-the-art performance in both SISR and Image Compression benchmarks, addressing limitations of previous methods.

**Limitations.** While the FIPER framework offers advances in image compression and super-resolution, it requires future work to accommodate computation-limited scenarios such as real-time decoding. Also, Factorized Fields don’t consider semantic information, and we will leave this to future research for more possibilities.



## References

- [1] Eirikur Agustsson and Radu Timofte. Ntire 2017 challenge on single image super-resolution: Dataset and study. In *The IEEE Conference on Computer Vision and Pattern Recognition (CVPR) Workshops*, 2017. 6
- [2] Johannes Ballé, David Minnen, Saurabh Singh, Sung Jin Hwang, and Nick Johnston. Variational image compression with a scale hyperprior. In *International Conference on Learning Representations*, 2018. 1, 7
- [3] Johannes Ballé, David Minnen, Saurabh Singh, Sung Jin Hwang, and Nick Johnston. Variational image compression with a scale hyperprior. In *International Conference on Learning Representations*, 2018. 2
- [4] Fabrice Bellard. The bpg image format. <http://bellard.org/bpg/>. Last accessed on 09/20/2015. 7
- [5] Marco Bevilacqua, Aline Roumy, Christine Guillemot, et al. Low-complexity single-image super-resolution based on nonnegative neighbor embedding. In *Proceedings of the British Machine Vision Conference (BMVC)*, pages 1–10, 2012. 6
- [6] Ang Cao and Justin Johnson. Hexplane: A fast representation for dynamic scenes. In *Proceedings of the IEEE/CVF Conference on Computer Vision and Pattern Recognition*, pages 130–141, 2023. 2, 3
- [7] Lahiru D. Chamain, Fabien Racapé, Jean Bégaint, Akshay Pushparaja, and Simon Feltman. End-to-end optimized image compression for machines, a study. In *2021 Data Compression Conference (DCC)*, 2021. 1, 2
- [8] Eric R. Chan, Connor Z. Lin, Matthew A. Chan, Koki Nagano, Boxiao Pan, Shalini De Mello, Orazio Gallo, Leonidas Guibas, Jonathan Tremblay, Sameh Khamis, Tero Karras, and Gordon Wetzstein. Efficient geometry-aware 3D generative adversarial networks. In *arXiv*, 2021. 2, 3
- [9] Anpei Chen, Zexiang Xu, Andreas Geiger, Jingyi Yu, and Hao Su. Tensorf: Tensorial radiance fields. In *European Conference on Computer Vision (ECCV)*, 2022.
- [10] Anpei Chen, Zexiang Xu, Xinyue Wei, Siyu Tang, Hao Su, and Andreas Geiger. Factor fields: A unified framework for neural fields and beyond. *arXiv preprint arXiv:2302.01226*, 2023. 2, 3, 4, 8
- [11] Fangdong Chen, Yumeng Xu, and Li Wang. Two-stage octave residual network for end-to-end image compression. In *Proceedings of the AAAI Conference on Artificial Intelligence*, 2022. 7
- [12] Hanting Chen, Yunhe Wang, Tianyu Guo, Chang Xu, Yiping Deng, Zhenhua Liu, Siwei Ma, Chunjing Xu, Chao Xu, and Wen Gao. Pre-trained image processing transformer. In *Proceedings of the IEEE/CVF conference on computer vision and pattern recognition*, pages 12299–12310, 2021. 1, 2, 7
- [13] Xiangyu Chen, Xintao Wang, Wenlong Zhang, Xiangtao Kong, Yu Qiao, Jiantao Zhou, and Chao Dong. Hat: Hybrid attention transformer for image restoration. *arXiv preprint arXiv:2309.05239*, 2023. 2, 6
- [14] Xiangyu Chen, Xintao Wang, Jiantao Zhou, Yu Qiao, and Chao Dong. Activating more pixels in image super-resolution transformer. In *Proceedings of the IEEE/CVF Conference on Computer Vision and Pattern Recognition (CVPR)*, pages 22367–22377, 2023. 4, 6, 7, 8
- [15] Z. Chen, Y. Zhang, J. Gu, L. Kong, X. Yang, and F. Yu. Dual aggregation transformer for image super-resolution. In *2023 IEEE/CVF International Conference on Computer Vision (ICCV)*, pages 12278–12287, 2023. 1, 2, 4, 6
- [16] Zheng Chen, Yulun Zhang, Jinjin Gu, Linghe Kong, and Xiaokang Yang. Recursive generalization transformer for image super-resolution. In *The Twelfth International Conference on Learning Representations*, 2024. 1, 2, 6
- [17] Zhongxue Cheng, Heming Sun, Masaru Takeuchi, and Jiro Katto. Learned image compression with discretized gaussian mixture likelihoods and attention modules. In *Proceedings of the IEEE/CVF conference on computer vision and pattern recognition*, pages 7939–7948, 2020. 1, 7
- [18] Yi-Shiuan Chou Chih-Chung Hsu, Chia-Ming Lee. Drct: Saving image super-resolution away from information bottleneck. *arXiv preprint arXiv:2404.00722*, 2023. 2, 6
- [19] Marcos V Conde, Ui-Jin Choi, Maxime Burchi, and Radu Timofte. Swin2SR: Swin2 transformer for compressed image super-resolution and restoration. In *Proceedings of the European Conference on Computer Vision (ECCV) Workshops*, 2022. 1, 2, 6
- [20] Jia Deng, Wei Dong, Richard Socher, Li-Jia Li, Kai Li, and Li Fei-Fei. Imagenet: A large-scale hierarchical image database. In *2009 IEEE Conference on Computer Vision and Pattern Recognition*, pages 248–255, 2009. 6
- [21] Chao Dong, Chen Change Loy, Kaiming He, and Xiaoou Tang. Image super-resolution using deep convolutional networks. *IEEE Transactions on Pattern Analysis and Machine Intelligence*, pages 295–307, 2014. 1, 2
- [22] Wenhong Duan, Zheng Chang, Chuanmin Jia, Shanshe Wang, Siwei Ma, Li Song, and Wen Gao. Learned image compression using cross-component attention mechanism. *IEEE Transactions on Image Processing*, 2023. 2, 4
- [23] Dahu Feng, Yan Huang, Yiwei Zhang, Jun Ling, Anni Tang, and Li Song. A generative compression framework for low bandwidth video conference. In *2021 IEEE International Conference on Multimedia & Expo Workshops (ICMEW)*, 2021. 2
- [24] Sara Fridovich-Keil, Giacomo Meanti, Frederik Rahbæk Warburg, Benjamin Recht, and Angjoo Kanazawa. K-planes: Explicit radiance fields in space, time, and appearance. In *Proceedings of the IEEE/CVF Conference on Computer Vision and Pattern Recognition*, pages 12479–12488, 2023. 2, 3
- [25] Dario Fuoli, Luc Van Gool, and Radu Timofte. Fourier space losses for efficient perceptual image super-resolution. In *Proceedings of the IEEE/CVF International Conference on Computer Vision*, pages 2360–2369, 2021. 3
- [26] Quankai Gao, Qiangeng Xu, Hao Su, Ulrich Neumann, and Zexiang Xu. Strivec: Sparse tri-vector radiance fields. In *Proceedings of the IEEE/CVF International Conference on Computer Vision*, pages 17569–17579, 2023. 2
- [27] Vivek K. Goyal. Theoretical foundations of transform coding. *IEEE Signal Processing Magazine*, 18(5):9–21, 2001. 1

- [28] Zongyu Guo, Zhizheng Zhang, Runsen Feng, and Zhibo Chen. Causal contextual prediction for learned image compression. *IEEE Transactions on Circuits and Systems for Video Technology*, 2022. 2
- [29] Wang Guo-Hua, Jiahao Li, Bin Li, and Yan Lu. EVC: Towards real-time neural image compression with mask decay. In *The Eleventh International Conference on Learning Representations*, 2023. 1
- [30] D. He, Z. Yang, W. Peng, R. Ma, H. Qin, and Y. Wang. Elic: Efficient learned image compression with unevenly grouped space-channel contextual adaptive coding. In *2022 IEEE/CVF Conference on Computer Vision and Pattern Recognition (CVPR)*, 2022. 2, 7
- [31] Jia-Bin Huang, Abhishek Singh, and Narendra Ahuja. Single image super-resolution from transformed self-exemplars. In *Proceedings of the IEEE Conference on Computer Vision and Pattern Recognition (CVPR)*, pages 5197–5206, 2015. 6
- [32] Wei Jiang, Jiayu Yang, Yongqi Zhai, Peirong Ning, Feng Gao, and Ronggang Wang. Mlic: Multi-reference entropy model for learned image compression. In *Proceedings of the 31st ACM International Conference on Multimedia*, pages 7618–7627, 2023. 7
- [33] Joint Video Experts Team (JVET). VVCSoftware\_VTM - VTM-21.2. [https://vcgit.hhi.fraunhofer.de/jvet/VVCSoftware\\_VTM/-/tree/VTM-21.2](https://vcgit.hhi.fraunhofer.de/jvet/VVCSoftware_VTM/-/tree/VTM-21.2), 2023. Accessed: 2023-10-23. 1
- [34] J. Kim, J. Lee, and K. Lee. Accurate image super-resolution using very deep convolutional networks. In *2016 IEEE Conference on Computer Vision and Pattern Recognition (CVPR)*, pages 1646–1654, 2016. 2
- [35] Alexander Kirillov, Eric Mintun, Nikhila Ravi, Hanzi Mao, Chloe Rolland, Laura Gustafson, Tete Xiao, Spencer Whitehead, Alexander C. Berg, Wan-Yen Lo, Piotr Dollár, and Ross Girshick. Segment anything. *arXiv:2304.02643*, 2023. 6
- [36] Cansu Korkmaz, A Murat Tekalp, and Zafer Dogan. Training generative image super-resolution models by wavelet-domain losses enables better control of artifacts. In *Proceedings of the IEEE/CVF Conference on Computer Vision and Pattern Recognition*, pages 5926–5936, 2024. 3
- [37] A. Burakhan Koyuncu, Han Gao, Atanas Boev, Georgii Gaikov, Elena Alshina, and Eckehard Steinbach. Contextformer: A transformer with spatio-channel attention for context modeling in learned image compression. In *Proceedings of the European Conference on Computer Vision (ECCV)*, 2022. 2
- [38] A Burakhan Koyuncu, Panqi Jia, Atanas Boev, Elena Alshina, and Eckehard Steinbach. Efficient contextformer: Spatio-channel window attention for fast context modeling in learned image compression. *IEEE Transactions on Circuits and Systems for Video Technology*, 2024. 2, 4
- [39] C. Ledig, L. Theis, F. Huszar, J. Caballero, A. Cunningham, A. Acosta, A. Aitken, A. Tejani, J. Totz, Z. Wang, and W. Shi. Photo-realistic single image super-resolution using a generative adversarial network. In *2017 IEEE Conference on Computer Vision and Pattern Recognition (CVPR)*, 2017. 1, 2
- [40] Christian Ledig, Lucas Theis, Ferenc Huszár, Jose Caballero, Andrew Cunningham, Alejandro Acosta, Andrew Aitken, Alykhan Tejani, Johannes Totz, Zehan Wang, et al. Photo-realistic single image super-resolution using a generative adversarial network. In *Proceedings of the IEEE conference on computer vision and pattern recognition*, pages 4681–4690, 2017. 2
- [41] A. Li, L. Zhang, Y. Liu, and C. Zhu. Feature modulation transformer: Cross-refinement of global representation via high-frequency prior for image super-resolution. In *2023 IEEE/CVF International Conference on Computer Vision (ICCV)*, 2023. 2
- [42] Daxin Li, Yuanchao Bai, Kai Wang, Junjun Jiang, Xianming Liu, and Wen Gao. Groupedmixer: An entropy model with group-wise token-mixers for learned image compression. *IEEE Transactions on Circuits and Systems for Video Technology*, 2024. 2, 4, 7
- [43] Wenbo Li, Xin Lu, Shengju Qian, Jiangbo Lu, Xiangyu Zhang, and Jiaya Jia. On efficient transformer-based image pre-training for low-level vision. *arXiv preprint arXiv:2112.10175*, 2021. 2
- [44] Jingyun Liang, Jiezhong Cao, Guolei Sun, Kai Zhang, Luc Van Gool, and Radu Timofte. Swinir: Image restoration using swin transformer. *arXiv preprint arXiv:2108.10257*, 2021. 2, 6
- [45] Bee Lim, Sanghyun Son, Heewon Kim, Seungjun Nah, and Kyoung Mu Lee. Enhanced deep residual networks for single image super-resolution. *2017 IEEE Conference on Computer Vision and Pattern Recognition Workshops (CVPRW)*, pages 1132–1140, 2017. 2
- [46] Bee Lim, Sanghyun Son, Heewon Kim, Seungjun Nah, and Kyoung Mu Lee. Enhanced deep residual networks for single image super-resolution. In *The IEEE Conference on Computer Vision and Pattern Recognition (CVPR) Workshops*, 2017. 1, 2, 6
- [47] Jie Liu, Wenjie Zhang, Yuting Tang, Jie Tang, and Gangshan Wu. Residual feature aggregation network for image super-resolution. In *Proceedings of the IEEE/CVF conference on computer vision and pattern recognition*, pages 2359–2368, 2020. 2
- [48] J. Liu, H. Sun, and J. Katto. Learned image compression with mixed transformer-cnn architectures. In *2023 IEEE/CVF Conference on Computer Vision and Pattern Recognition (CVPR)*. IEEE Computer Society, 2023. 1, 2, 5, 7, 8
- [49] Jinming Liu, Heming Sun, and Jiro Katto. Learned image compression with mixed transformer-cnn architectures. In *Proceedings of the IEEE/CVF Conference on Computer Vision and Pattern Recognition*, pages 14388–14397, 2023. 7
- [50] Ze Liu, Yutong Lin, Yue Cao, Han Hu, Yixuan Wei, Zheng Zhang, Stephen Lin, and Baining Guo. Swin transformer: Hierarchical vision transformer using shifted windows. In *Proceedings of the IEEE/CVF international conference on computer vision*, pages 10012–10022, 2021. 2
- [51] Ze Liu, Han Hu, Yutong Lin, Zhuliang Yao, Zhenda Xie, Yixuan Wei, Jia Ning, Yue Cao, Zheng Zhang, Li Dong, et al. Swin transformer v2: Scaling up capacity and resolution. In

- Proceedings of the IEEE/CVF conference on computer vision and pattern recognition*, pages 12009–12019, 2022. 4
- [52] I Loshchilov. Decoupled weight decay regularization. *arXiv preprint arXiv:1711.05101*, 2017. 7
- [53] Qi Mao, Tinghan Yang, Yinuo Zhang, Shuyin Pan, Meng Wang, Shiqi Wang, and Siwei Ma. Extreme image compression using fine-tuned vqgan models. 2023. 2
- [54] Qi Mao, Tinghan Yang, Yinuo Zhang, Shuyin Pan, Meng Wang, Shiqi Wang, and Siwei Ma. Extreme image compression using fine-tuned vqgan models. *ArXiv*, 2023. 2
- [55] D Martin, C Fowlkes, D Tal, et al. A database of human segmented natural images and its application to evaluating segmentation algorithms and measuring ecological statistics. In *Proceedings of the IEEE International Conference on Computer Vision (ICCV)*, pages 416–423, 2001. 6
- [56] Yusuke Matsui, Koichi Ito, Yuki Aramaki, et al. Sketch-based manga retrieval using manga109 dataset. *Multimedia Tools and Applications*, 76(20):21811–21838, 2017. 6
- [57] David Minnen and Saurabh Singh. Channel-wise autoregressive entropy models for learned image compression. In *2020 IEEE International Conference on Image Processing (ICIP)*, pages 3339–3343, 2020. 7
- [58] David Minnen, Johannes Ballé, and George D Toderici. Joint autoregressive and hierarchical priors for learned image compression. *Advances in neural information processing systems*, 31, 2018. 1
- [59] Thomas Müller, Alex Evans, Christoph Schied, and Alexander Keller. Instant neural graphics primitives with a multiresolution hash encoding. *ACM Trans. Graph.*, 41(4):102:1–102:15, 2022. 2, 3
- [60] Maxime Oquab, Timothée Darcet, Theo Moutakanni, Huy V. Vo, Marc Szafraniec, Vasil Khalidov, Pierre Fernandez, Daniel Haziza, Francisco Massa, Alaaeldin El-Nouby, Russell Howes, Po-Yao Huang, Hu Xu, Vasu Sharma, Shang-Wen Li, Wojciech Galuba, Mike Rabbat, Mido Assran, Nicolas Ballas, Gabriel Synnaeve, Ishan Misra, Herve Jegou, Julien Mairal, Patrick Labatut, Armand Joulin, and Piotr Bojanowski. Dinov2: Learning robust visual features without supervision, 2023. 5
- [61] Chenyang Qi, Xin Yang, Ka Leong Cheng, Ying-Cong Chen, and Qifeng Chen. Real-time 6k image rescaling with rate-distortion optimization. In *Proceedings of the IEEE/CVF Conference on Computer Vision and Pattern Recognition (CVPR)*, 2023. 7
- [62] Oren Rippel and Lubomir Bourdev. Real-time adaptive image compression. In *Proceedings of the 34th International Conference on Machine Learning (PMLR)*, 2017. 2
- [63] Juan Song, Jiayang He, Mingtao Feng, Keyan Wang, Yunsong Li, and Ajmal Mian. High frequency matters: Uncertainty guided image compression with wavelet diffusion. *arXiv preprint arXiv:2407.12538*, 2024. 2, 4
- [64] Long Sun, Jinshan Pan, and Jinhui Tang. Shufflemixer: An efficient convnet for image super-resolution. In *Advances in Neural Information Processing Systems*, pages 17314–17326, 2022. 2
- [65] Ying Tai, Jian Yang, and Xiaoming Liu. Image super-resolution via deep recursive residual network. In *Proceedings of the IEEE conference on computer vision and pattern recognition*, pages 3147–3155, 2017. 2
- [66] David Taubman and Michael Marcellin. *JPEG2000 Image Compression Fundamentals, Standards and Practice*. Springer Publishing Company, Incorporated, 2013. 1, 2
- [67] Joint Video Experts Team. Vvc official test model vtm. 2021. 7
- [68] Tong Tong, Gen Li, Xiejie Liu, and Qinquan Gao. Image super-resolution using dense skip connections. In *Proceedings of the IEEE international conference on computer vision*, pages 4799–4807, 2017. 2
- [69] G.K. Wallace. The jpeg still picture compression standard. *IEEE Transactions on Consumer Electronics*, 38(1):xviii–xxxiv, 1992. 1, 2, 7
- [70] Xintao Wang, Ke Yu, Shixiang Wu, Jinjin Gu, Yihao Liu, Chao Dong, Yu Qiao, and Chen Change Loy. Esrgan: Enhanced super-resolution generative adversarial networks. In *Computer Vision – ECCV 2018 Workshops*, 2019. 2
- [71] Xintao Wang, Liangbin Xie, Chao Dong, and Ying Shan. Real-esrgan: Training real-world blind super-resolution with pure synthetic data. In *2021 IEEE/CVF International Conference on Computer Vision Workshops (ICCVW)*, 2021. 2
- [72] H. Wu, B. Xiao, N. Codella, M. Liu, X. Dai, L. Yuan, and L. Zhang. Cvt: Introducing convolutions to vision transformers. In *2021 IEEE/CVF International Conference on Computer Vision (ICCV)*, 2021. 2
- [73] Yueqi Xie, Ka Leong Cheng, and Qifeng Chen. Enhanced invertible encoding for learned image compression. In *Proceedings of the ACM International Conference on Multimedia*, pages 162–170, 2021. 7
- [74] R Zeyde, M Elad, and M Protter. On single image scale-up using sparse-representations. In *Proceedings of the International Conference on Curves and Surfaces (ICCS)*, pages 711–730, 2010. 6
- [75] Leheng Zhang, Yawei Li, Xingyu Zhou, Xiaorui Zhao, and Shuhang Gu. Transcending the limit of local window: Advanced super-resolution transformer with adaptive token dictionary. In *Proceedings of the IEEE/CVF Conference on Computer Vision and Pattern Recognition*, pages 2856–2865, 2024. 2, 4, 6
- [76] Leheng Zhang, Yawei Li, Xingyu Zhou, Xiaorui Zhao, and Shuhang Gu. Transcending the limit of local window: Advanced super-resolution transformer with adaptive token dictionary. In *Proceedings of the IEEE/CVF Conference on Computer Vision and Pattern Recognition*, pages 2856–2865, 2024. 6
- [77] Yulun Zhang, Kunpeng Li, Kai Li, Lichen Wang, Bineng Zhong, and Yun Fu. Image super-resolution using very deep residual channel attention networks. In *Proceedings of the European Conference on Computer Vision (ECCV)*, 2018. 2
- [78] Yulun Zhang, Yapeng Tian, Yu Kong, Bineng Zhong, and Yun Fu. Residual dense network for image super-resolution. In *Proceedings of the IEEE conference on computer vision and pattern recognition*, pages 2472–2481, 2018. 2
- [79] Shangchen Zhou, Jiawei Zhang, Wangmeng Zuo, and Chen Change Loy. Cross-scale internal graph neural network for image super-resolution. *Advances in neural information processing systems*, 33:3499–3509, 2020. 2

- [80] Qiang Zhu, Pengfei Li, and Qianhui Li. Attention retractable frequency fusion transformer for image super resolution. In *Proceedings of the IEEE/CVF Conference on Computer Vision and Pattern Recognition*, pages 1756–1763, 2023. [2](#)
- [81] Yin hao Zhu, Yang Yang, and Taco Cohen. Transformer-based transform coding. In *International Conference on Learning Representations*, 2022. [2](#)
- [82] Renjie Zou, Chunfeng Song, and Zhaoxiang Zhang. The devil is in the details: Window-based attention for image compression. In *CVPR*, 2022. [7](#)